Take Me Home: Reversing Distribution Shifts using Reinforcement Learning

Vivian Lin **Kuk Jang** **Souradeep Dutta** **Michele Caprio** **Oleg Sokolsky** **Insup Lee**

PRECISE Center, University of Pennsylvania, Philadelphia, PA 19104, USA

arXiv:2302.10341v1 [cs.LG] 20 Feb 2023

Abstract

Deep neural networks have repeatedly been shown to be non-robust to the uncertainties of the real world. Even subtle adversarial attacks and naturally occurring distribution shifts wreak havoc on systems relying on deep neural networks. In response to this, current state-of-the-art techniques use data-augmentation to enrich the training distribution of the model and consequently improve robustness to natural distribution shifts. We propose an alternative approach that allows the system to recover from distribution shifts online. Specifically, our method applies a sequence of semantic-preserving transformations to bring the shifted data closer in distribution to the training set, as measured by the Wasserstein distance. We formulate the problem of sequence selection as an MDP, which we solve using reinforcement learning. To aid in our estimates of Wasserstein distance, we employ dimensionality reduction through orthonormal projection. We provide both theoretical and empirical evidence that orthonormal projection preserves characteristics of the data at the distributional level. Finally, we apply our distribution shift recovery approach to the ImageNet-C benchmark for distribution shifts, targeting shifts due to additive noise and image histogram modifications. We demonstrate an improvement in average accuracy up to 14.21% across a variety of state-of-the-art ImageNet classifiers.

1 INTRODUCTION

The brittleness of deep learning models remains a difficult challenge. Even with their successful deployment to many application domains, it has only grown more important to determine and improve the robustness of approaches using deep learning. Some efforts to prevent such failures focus on the adversarial setting for model robustness, studying the worst case accuracy of classifiers. However, these scenarios are unlikely to occur in the real world. A more realistic challenge is when *naturally* occurring shifts take place. In Hendrycks and Dietterich [2019], a set of commonly occurring shifts were proposed as a benchmark dataset. These disturbances are *semantic-preserving* shifts in the sense that the underlying meaning or label that a model must predict is unchanged, despite the corruption to the input. This paper focuses on robustness to such naturally-occurring shifts.

Many state-of-the-art techniques have addressed the issue of robustness towards semantic-preserving shifts. The most common approaches use data augmentation techniques to generate samples with noise disturbances. AugMix [Hendrycks et al., 2019] applies a set of transformations (e.g., rotation, translation, shear, etc.) to distort the original image. NoisyMix [Erichson et al., 2022] takes this augmentation one step further by injecting noises into the augmented examples, expanding the experiences that a model would be exposed to during training. ManifoldMix [Verma et al., 2019] also uses a data augmentation approach, but focuses on generating examples from a lower-dimensional latent manifold. Other notable work in the recent literature includes CutMix [Yun et al., 2019], PuzzleMix [Kim et al., 2020], and DeepAugment [Hendrycks et al., 2020].

In contrast, we propose an online technique that exploits the following observation: when distribution shift arises in the external environment due to natural causes, it persists for a certain duration of time. For instance, when a corruption in image quality occurs due to snow, this corruption does not disappear in the next image frame. This gives the system some time to *adapt* and *recover* from this shift by computing some semantic preserving transformations to the data.

We propose a technique, Supervisory system for Shift Adaptation and Recovery (`SuperStAR`), that learns to apply a set of semantic-preserving transforms, correcting the input to align with the original training set of the classifier. This allows the system to recover from distribution shifts

online. Moreover, this approach can be used in conjunction with other DNN directed techniques like data-augmentation schemes to improve their performance.

Additionally, our approach uses a lower-dimensional approximation of the Wasserstein distance to navigate the process of shift correction. As with image classification, models often operate on high-dimensional input spaces. This presents a challenge when employing statistical distance measures, such as the Wasserstein distance, to measure the distance between the training set of images and the set of images a model encounters during deployment. Recently, results by Cai and Lim [2022] have shown a method for measuring distances between distributions of different dimension, inspiring our dimensionality reduction approach.

We summarize our contributions in order to address the problem of robustness to semantic-preserving shifts:

1. We develop an approach for distribution shift correction using reinforcement learning.
2. We develop a method to efficiently compute the degree of distribution shift by projecting to a lower dimensional space. This uses results from Cai and Lim [2022] in conjunction with the Wasserstein distance.
3. We demonstrate an application to Imagenet-C, targeting shifts due to additive noise and image histogram modifications. Our empirical results show significant accuracy improvements (up to 14.21% averaged across all shift severity levels) on top of standard training and data-augmentation schemes.

2 PRELIMINARIES

We begin by assuming that the images are sampled from a measurable space $(\mathcal{X}, \mathcal{A}_{\mathcal{X}})$. $\mathcal{X}$ is usually decided by the image format, but it is a countable subset of the Euclidean space $\mathbb{R}^{h\times w\times 3}$, where h, w denote the height and width of the image, respectively, and the third dimension encodes the color information. Let $\Delta(\mathcal{X}, \mathcal{A}_{\mathcal{X}})$ denote the set of all probability measures on $(\mathcal{X}, \mathcal{A}_{\mathcal{X}})$. We pick a distribution $D \in \Delta(\mathcal{X}, \mathcal{A}_{\mathcal{X}})$ from which the current set of images are sampled. Additionally, let us assume that the labels belong to a measurable space $(\mathcal{Y}, \mathcal{A}_{\mathcal{Y}})$, and a classifier C is an $\mathcal{A}_{\mathcal{X}}\backslash\mathcal{A}_{\mathcal{Y}}$ measurable map, $\mathcal{C} : \mathcal{X} \to \mathcal{Y}$. An *oracle classifier* $\mathcal{C}^*$ produces the ground truth labels. Next, we define a semantic preserving transform $\mathbb{T}$.

Definition 2.1 (Semantic Preserving Transform)**.** A function $\mathbb{T} : \mathcal{X} \to \mathcal{X}$ is semantic preserving iff $\mathcal{C}^*(x) = \mathcal{C}^*(\mathbb{T}(x))$, for all $x \in \mathcal{X}$

We denote by $\mathbb{S}$ the set of all such semantic preserving transforms. In the standard ERM paradigm, we approximate $\mathcal{C}^*$ with some classifier $\mathcal{C}$. When measuring robustness to common corruptions, typically a corrupting transform $\mathbb{T}_c$ belongs to $\mathbb{S}$. This includes transforms like addition of Gaussian noise, speckle noise and alike. The error of a classifier $\mathcal{C}$ under the distribution D, is defined as

$$err(D) := \mathbb{E}_{x\sim D}\left[\mathbb{1}(\mathcal{C}^*(x) \neq \mathcal{C}(x))\right],$$

where $\mathbb{1}$ is the standard indicator function, which evaluates to 1 iff $\mathcal{C}^*(x) \neq \mathcal{C}(x)$.[1] For a robust classifier we expect $err(D)$ to be minimal, for different choices of the distribution D. For instance in the case of common corruptions introduced in Hendrycks and Dietterich [2019], the goal is to optimize the choice of classifier $\mathcal{C}$ such that $err(D)$ is minimized. This is typically achieved using data-augmentation schemes such as Augmix, NoisyMix, and DeepAugment.

3 PROBLEM STATEMENT AND APPROACH

Note that a semantic preserving transform $\mathbb{T}$ is generally not invertible. Consider a random variable x_c such that $x_c = \mathbb{T}(z)$, where $z \sim D$. Let us denote the distribution of x_c by $D_{\mathbb{T}}$. It is hard to undo the corruption, even with full knowledge of the transform, except in the simplest of cases such as when $\mathbb{T}$ is a brightness transform. In practice, it might be possible to choose an element $\mathbb{T}'$ from the set of semantic preserving transforms $\mathbb{S}$ such that it is possible to partially recover the accuracy drop due to $\mathbb{T}$. In fact it might be better to expand from a single inverse transform, to a sequence of transforms from $\mathbb{S}$. That is an ordered set $\mathcal{T} := \{\mathbb{T}_k, \mathbb{T}_{k-1}, \dots \mathbb{T}_1\}$ with $k \geq 1$, such that $\mathbb{S} \ni \mathcal{I}_k(x) := \mathbb{T}_k \circ \mathbb{T}_{k-1} \circ \cdots \circ \mathbb{T}_1(x)$.[2] Ideally, we wish to find an algorithm which optimizes the following:

$$\begin{aligned} \mathcal{I}_k^* &= \operatorname*{argmin}_{\mathcal{I}_k} R(\mathcal{I}_k), \\ R(\mathcal{I}_k) &= err(D_{\mathcal{I}_k\circ\mathbb{T}}) - err(D), \end{aligned} \tag{1}$$

where $D_{\mathcal{I}_k\circ\mathbb{T}}$ denotes the distribution of $\mathcal{I}_k \circ \mathbb{T}(z)$, $z \sim D$. The transform $\mathcal{I}_k$ is what effectively *reverses* an image corruption due to $\mathbb{T}$.

Approach. We present an overview of our `SuperStAR` algorithm here. At a high level its functioning is akin to a supervisor for the classifier shown in Figure 1. `SuperStAR` detects distribution shifts, and computes a recovery strategy to be applied before sending an image to a classifier. We make the following assumptions. At training time the algorithm has access to a validation set $\mathbf{V} = \{v_1, \dots, v_n\}$, where v_i is drawn i.i.d from the training distribution D. At inference time it has access to a corrupted set $\mathbf{V}_c = \{v_1^c, v_2^c, \dots, v_n^c\}$, where v_i^c is drawn i.i.d from $D_{\mathbb{T}_c}$, $\mathbb{T}_c \in \mathbb{S}$. Using $\mathbf{V}$ and $\mathbf{V}_c$, `SuperStAR` constructs the transform $\mathcal{I}_k^*$. We propose a two-fold process to achieve this.

[1] For notational convenience, we hereafter denote both a random variable and its realization by a lowercase Latin letter.

[2] The order $\prec_{\mathcal{T}}$ on $\mathcal{T}$ is given by $\mathbb{T}_i \prec_{\mathcal{T}} \mathbb{T}_j \iff i < j$, $i, j \in \mathbb{N}$. In addition, $\mathbb{T}_0$ is assumed to be the identity function.

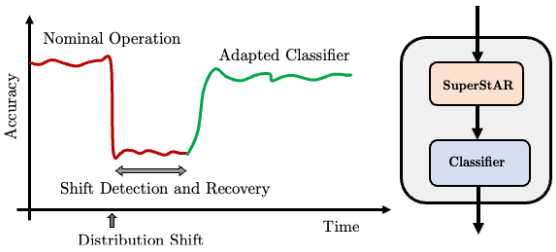

Figure 1: Overview of SuperStAR for distribution shift detection and recovery. At deployment, assume that a distribution shift causes a drop in accuracy. This is detected through changes in the Wasserstein distance between the validation set $\mathbf{V}$ of images and the corrupted set $\mathbf{V}_c$. SuperStAR computes a composition of transforms $\mathcal{I}_k$ to adapt to the shift and recover accuracy. SuperStAR composes with a base classifier to detect and adapt to distribution shifts, increasing the robustness of classification.

4 DETECTION AND CORRECTION

Deployment. We refer the reader to Figure 1. At deployment, when the system detects a shift in distribution compared to a clean validation set, it proposes a composition of transforms $\mathcal{I}_k$. From the vantage point of classifier $\mathcal{C}$, images transformed using $\mathcal{I}_k$ *appear* to be closer to the *home* distribution D. The effectiveness of this candidate transform is judged using Wasserstein distance from a validation set. We describe this in detail later in the Section.

Design Time. At design time, we train a deep neural network policy π such that, given a corrupted set $\mathbf{V}_c$ of i.i.d observations from corrupted distribution D_c, the policy generates a finite composition $\mathcal{I}_k$ of $k < \infty$ transforms from $\mathbb{S}$ that solves the optimization problem in Equation 1. This is described in detail in Section 5.

As mentioned, the SuperStAR algorithm has access to a validation set $\mathbf{V}$ drawn i.i.d. from D. In the presence of a shift incurred by $\mathbb{T}$, it samples a corrupted set $\mathbf{V}_c$ from $D_{\mathbb{T}}$ and selects $\mathcal{T} := \{\mathbb{T}_k, \mathbb{T}_{k-1}, \ldots \mathbb{T}_1\}$ using a policy π. We fix a maximum horizon k to keep the algorithm tractable at both learning and deployment. The procedure for selecting sequence $\mathcal{T}$ is presented in Algorithm 1. In Line 1, Algorithm 1 first uses the estimator $\tilde{W}$ to estimate the initial Wasserstein distance. Next, it runs policy π for k steps (Lines $4-11$), where it iteratively applies the transform picked by the policy to update the corrupted set. The algorithm uses a lower dimensional state representation of $\mathbf{V}$ for evaluating the policy and for the estimator $\tilde{W}$ (discussed in more detail in Section 5). The algorithm collects this set of transforms in T and returns the sequence. The stopping criterion in Line 8 guards against two phenomena. First, it avoids overly transforming images to a point of diminishing returns. Second, a more practical reason, it hedges against the chance that the distribution shift is not semantic preserving, which is always possible in reality. In the worst case, images from a completely unknown class or faulty hardware could destroy semantics. Hence, we pause the policy when the Wasserstein distance decreases within a threshold.

Algorithm 1 Transformation Selection

Input: Validation set $\mathbf{V}$, corrupted set $\mathbf{V}_c$, policy π, horizon k, thresholds $\alpha, \beta \in (0, 1]$

1: $w_0 \leftarrow \tilde{W}(\mathbf{V}, \mathbf{V}_c)$, $\mathbf{V}_0 \leftarrow \mathbf{V}_c$, $T \leftarrow \{\ \}$
2: **for** $i = 1, \ldots, k$ **do**
3: $\quad \mathbb{T}_i \leftarrow \pi(\mathbf{V}_{i-1})$
4: $\quad \mathbf{V}_i \leftarrow \mathbb{T}_i(\mathbf{V}_{i-1})$
5: $\quad w_i \leftarrow \tilde{W}(\mathbf{V}, \mathbf{V}_i)$
6: $\quad$ **if** $w_i \leq \alpha\, w_0 \vee w_i \geq \beta\, w_{i-1}$ **then**
7: $\quad\quad$ Return T
8: $\quad$ **end if**
9: $\quad T \leftarrow \{\mathbb{T}_i\} \cup T$
10: **end for**
11: Return T

5 TRAINING RECOVERY POLICY USING REINFORCEMENT LEARNING

Our task is to compute a composition of transforms $\mathcal{I}_k$ to apply to the set $\mathbf{V}_c$, sampled i.i.d from D_c, to realize the optimization cost outlined in Equation 1. To this end, we note the following theorem.

Theorem 5.1. *$R(\mathcal{I}_k) \leq \alpha \cdot d_{TV}(D, D_{\mathcal{I}_k \circ \mathbb{T}})$, for some finite $\alpha \in \mathbb{R}$ and semantic preserving transform $\mathcal{I}_k$.*

Proof: See Section A of Supplementary Material. □

Thus, for a transform $\mathbb{T}$ (possibly a corruption), it is possible for the classifier to recover performance if the apparent distribution under $\mathcal{I}_k \circ \mathbb{T}$ is close enough to the original distribution D. We set up the search of $\mathcal{I}_k$ as a reinforcement learning problem. The agent attempts to maximize its rewards, measured as the inverse of distance from D. To achieve this it uses *actions*, which are semantic preserving transforms designed to correct the effects of a corruption.

5.1 MDP FORMULATION

Definition 5.2 (MDP). A *Markov Decision Process (MDP)* is a 6-tuple $\mathcal{E} = (\mathcal{S}, \mathbb{A}, \mathcal{P}, \mathcal{R}, \gamma, \mathrm{I}_0)$, where $\mathcal{S} \subseteq \mathbb{R}^n$ is the set of states, $\mathbb{A} \subseteq \mathbb{R}^m$ is the set of actions, $\mathcal{P}(s'|s, a)$ specifies the probability of transitioning from state s to s' on action a, $\mathcal{R}(s, a)$ is the reward returned when taking action a from state s, $\gamma \in [0, 1)$ is the discount factor, and I_0 is the initial state distribution.

In the following, we formulate the task of computing $\mathcal{I}_k$ as obtaining a reactive policy for an MDP. We first walk through the realizations of the different components.

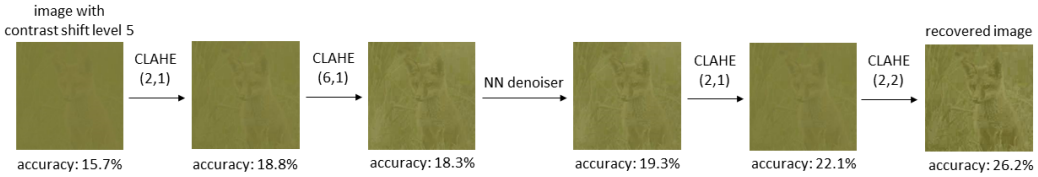

Figure 2: Example of transformations applied to a corrupted image of constrast shift level 5. CLAHE(x,y) denotes histogram equalization with strength determined by x and y (further description can be found in Section 8). The policy learns to apply a non-trivial composition of transformations that would be difficult to find through manual manipulation. The policy chooses few redundant actions and improves the accuracy of an AugMix-trained ResNet-50 on a random batch of 1000 images.

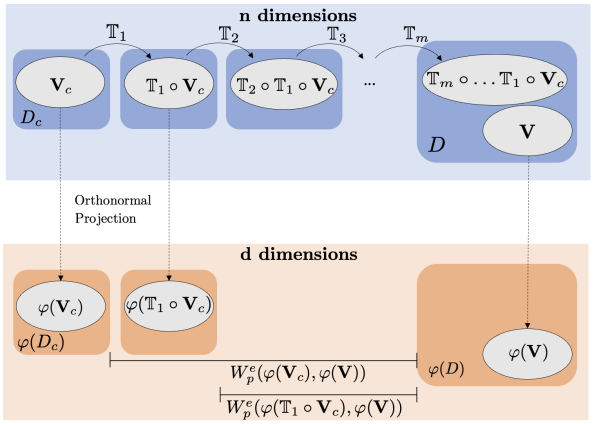

Figure 3: Operation of `SuperStAR` . Starting from $\mathbf{V}_c$, the algorithm selects a sequence of transforms $\mathcal{T}$ which move $\mathbf{V}_c$ closer to the original distribution $\mathbf{V}$. During the sequence, the orthonormal projections $\varphi(\mathbf{V})$ and $\varphi(\mathbf{V}_c)$ are used to compute the Wasserstein distance $W_p(\varphi(\mathbf{V}_c), \varphi(\mathbf{V}))$. See Sec. 6 for details.

State Representation. The environment has access to a set $\mathbf{V} \subset \mathcal{X}$, which is a set of possibly corrupted images. A state of the MDP is a compressed representation of the above set $\mathbf{V}$ encapsulating the type of corruptions subjected to an image. Let us assume that this projection is captured by some function $\mathbb{F}_R : \mathcal{A}_\mathcal{X} \to \mathfrak{R}$, where $\mathfrak{R}$ is the space of representations for a set of images. For a representation $r = \mathbb{F}_R(\mathbf{V})$, we want it to be rich enough that a policy can decipher the appropriate choice of action in $\mathbb{A}$, but also compact enough that it is possible to learn a policy within a few episodes. Typically, a smaller state space size leads to faster convergence for reinforcement learning algorithms.

In this paper, for a set of images $\mathbf{V}$, we select a 3-dimensional state representation that measures the average brightness, standard deviation, and entropy of the images in $\mathbf{V}$. First, we preprocess the images into its grayscale values. Next, for each image we obtain the discrete wavelet transform and compute its average brightness, standard deviation and entropy. The state representation is finally an average of all these values across the images,

$$\mathbb{F}_R(\mathbf{V}) = \frac{1}{|\mathbf{V}|} \sum_{x \in \mathbf{V}} \left[AvgBri_x, \quad StDev_x, \quad Entr_x \right]^\top, \tag{2}$$

where, $AvgBri_x, StDev_x, Entr_x \in \mathbb{R}$ are the average brightness, standard deviation, and entropy of an image x, respectively.

Actions. The set of actions $\mathbb{A} \subseteq \mathbb{S}$ is a set of semantic preserving transforms from which the learner chooses to maximize some reward. Hence, capturing Equation 1 as a reward leads the agent to pick actions that mitigate the current corruption to some extent.

Transitions. The idea of transitions in this case is to model the effect of applying a transform from $\mathbb{S}$ to a possibly corrupted set $\mathbf{V}_c$. With slight abuse of notation, we use $\mathbb{T}(\mathbf{V})$ to denote set $\{v' : v' = \mathbb{T}(v), v \in \mathbf{V}\}$.

Computing Reward. As shown in Figure 3, computing the reward for a set of images $\mathbf{V}_c$ corresponds to measuring the distance from a clean validation set $\mathbf{V}$. Ideally, the distance between the distributions from which $\mathbf{V}_c$ and $\mathbf{V}$ are drawn would be measured, but this is difficult without knowledge of the source distributions. Instead, we use an empirical estimate of Wasserstein distance [Bonneel et al., 2011] to compute the distributional distance between sets $\mathbf{V}_c$ and $\mathbf{V}$.

In practice the policy might not be able to reduce the W_p^e to a level such that the classifier completely recovers the loss in accuracy. One reason for this is the possible non-existence of the inverse of the corruption transform in $\mathbb{S}$. Another is that, while a transformation may reduce W_p^e, it may also overly alter the image content such that the classifier performs poorly. Ideally, we can combat against this by ensuring that actions make incremental changes to the image. However, this is hard to control. We therefore add a regularizer to the above Wasserstein distance that penalizes excessive changes to the image. We use a measure of image similarity known as $ssim$ [Wang et al., 2004] which computes the visual similarity between pairs of images. Given $\lambda > 0$ and $0 \leq \omega < 1$, the reward function is given by

$$\begin{aligned} R(s_t, a_t) = &-W_p^e(\mathbf{V}, \mathbb{F}_R^{-1}(s_t)) \\ &+ \lambda L_S(\mathbb{F}_R^{-1}(s_0), \mathbb{F}_R^{-1}(s_{t+1})), \end{aligned} \tag{3}$$

where

$$L_S(\mathbf{X}, \mathbf{Y}) = \begin{cases} \log(1 - ssim(\mathbf{X}, \mathbf{Y})), & ssim(\mathbf{X}, \mathbf{Y}) < \omega \\ 0 & \text{otherwise.} \end{cases} \tag{4}$$

Initial State. At test time, the initial state of the MDP is

produced by a random environment corruption from the set $\mathbb{S}$ that the system is subjected to. In reality the designer does not have access to any of these corrupting transforms. Hence, at training time we train a policy network to reverse a set of *surrogate* corruptions from $\mathbb{S}$, with the hope that some of these transfer at inference time to an unseen set of corruptions. We explain the details of the surrogate corruptions in Section 8. We pick uniformly randomly from a finite set of $\mathsf{S}_c \subset \mathbb{S}$ of these surrogate corruptions to sample the initial state I_0.

5.2 LEARNING ALGORITHM

A policy $\pi : \mathcal{S} \to \mathbb{A}$ for the MDP $\mathcal{E}$ is a strategy to recover the distribution shift. The value of a state for policy π is the expected return $\mathbf{R}_\pi(s_0)$, starting from state s_0, while executing the policy π at every step, $a_t = \pi(s_t)$. The optimal policy π^* maximizes the reward starting from the initial state distribution – i.e., $\pi^* = \arg\max V^{\mathrm{I}_0}(\pi)$, where $V^{\mathrm{I}_0}(\pi) = \mathbb{E}_{s_0 \in \mathrm{I}_0}[\mathbf{R}_\pi(s_0)]$.

6 ORTHONORMAL PROJECTIONS FOR DIMENSIONALITY REDUCTION

In this section, we discuss the practical constraints of estimating the Wasserstein distance in high dimensions. Further, to mitigate these concerns, we examine dimensionality reduction through orthonormal projection as a means of improving the sample efficiency of this estimate.

The empirical estimate of the Wasserstein distance converges in sample size to the true Wasserstein distance slowly in large dimensions [Ramdas et al., 2017]. This suggests that, ideally, by reducing the dimensionality of the sample data, fewer samples are needed to achieve an accurate estimate of the Wasserstein distance. Naturally, the efficacy of such a technique is contingent on minimal loss of information incurred by the dimensionality reduction. We posit that orthonormal projection is a reduction technique that preserves characteristics of the sample data at a distributional level. An intuitive motivation for this arises from a metric we refer to as the *Cai-Lim distance* [Cai and Lim, 2022].

Let $m, n \in \mathbb{N}$ and $p \in [1, \infty]$. Call $M(\mathbb{R}^n)$ and $M(\mathbb{R}^m)$ the spaces of probability measures on $\mathbb{R}^n$ and $\mathbb{R}^m$, respectively. Denote then by $M^p(\mathbb{R}^n)$ and $M^p(\mathbb{R}^m)$ the spaces of probability measures having finite p-th moment on $\mathbb{R}^n$ and $\mathbb{R}^m$, respectively (here $p = \infty$ is interpreted in the limiting sense of essential supremum). For convenience, we consider only probability measures with densities, so that we do not have to keep track of which measure is absolutely continuous to which other measure [Cai and Lim, 2022, Section III].

Suppose now $m \leq n$ and consider the Stiefel manifold on of $m \times n$ matrices with orthonormal rows.

$$O(m, n) := \{V \in \mathbb{R}^{m \times n} : VV^\top = I_d\}.$$

For any $V \in O(m, n)$ and $b \in \mathbb{R}^m$, let

$$\varphi_{V,b} : \mathbb{R}^n \to \mathbb{R}^m, \quad x \mapsto \varphi_{V,b}(x) := Vx + b,$$

and for any $\mu \in M(\mathbb{R}^n)$, let $\varphi_{V,b}(\mu) := \mu \circ \varphi_{V,b}^{-1}$ be the pushforward measure. This can be seen as a projection of μ onto the smaller dimensional space $\mathbb{R}^m$, and we call it a *Cai-Lim projection*; it is not unique: it depends on the choice of V and b. Recall then the definition of the p-Wasserstein distance between $\mu, \nu \in M^p(\mathbb{R}^n)$:

$$W_p(\mu, \nu) := \left[\inf_{\gamma \in \Gamma(\mu,\nu)} \int_{\mathbb{R}^{2n}} \|x - y\|_2^p \, \mathrm{d}\gamma(x, y) \right]^{\frac{1}{p}},$$

where $\| \cdot \|_2$ denotes the Euclidean norm and

$$\Gamma(\mu, \nu) := \{\gamma \in M(\mathbb{R}^{2n}) : \pi_1^n(\gamma) = \nu, \pi_2^n(\gamma) = \mu\}$$

is the set of couplings between μ and ν, where π_1^n is the projection onto the first n coordinates and π_2^n is the projection onto the last n coordinates.

Denote by

$$\Phi^-(\mu, d) := \{\beta \in M(\mathbb{R}^m) : \varphi_{V,b}(\mu) = \beta, \text{ for some } V \in O(d, n), b \in \mathbb{R}^m\}.$$

the set of Cai-Lim projections of μ onto $\mathbb{R}^m$. We call *Cai-Lim distance* between $\mu \in M^p(\mathbb{R}^n)$ and $\nu \in M^p(\mathbb{R}^m)$, $m \leq n$, the smallest p-Wasserstein distance between ν and a Cai-Lim projection of μ onto $\mathbb{R}^m$, for some $p \in [1, \infty]$. That is,

$$W_p^{CL}(\mu, \nu) := \inf_{\beta \in \Phi^-(\mu,d)} W_p(\beta, \nu). \tag{5}$$

We note that *Cai-Lim distance* is closely related to Monge and Kantorovich's formulations of the optimal transport problem (see Section B of Supplementary Material). A generalization of the Wasserstein distance, the Cai-Lim distance allows for measurements of distance between distributions of different dimensions. It follows directly from (5) that when an orthonormal projection is applied, $\nu = \varphi_{V,0}(\mu)$, the Cai-Lim distance is trivially zero, $W_p^{CL}(\mu, \nu) = 0$. This suggests that the orthonormal projection preserves information about the distance between two distributions.

We now present more rigorous theoretical justification of this claim. The following is an important result.

Lemma 6.1. ***([Cai and Lim, 2022, Lemma II.1])*** *Let $m, n \in \mathbb{N}$ and $p \in [1, \infty]$, and assume $m \leq n$. For any $\mu, \nu \in M^p(\mathbb{R}^n)$, any $V \in O(m, n)$, and any $b \in \mathbb{R}^m$, we have that*

$$W_p(\varphi_{V,b}(\mu), \varphi_{V,b}(\nu)) \leq W_p(\mu, \nu).$$

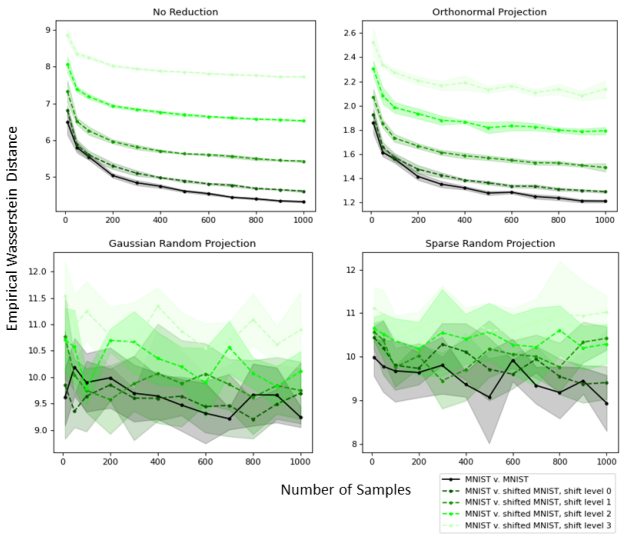

Figure 4: Empirical Wasserstein distance between MNIST and MNIST with varied levels of additive Gaussian noise, over a range of sample sizes. Curves are over 5 trials. MNIST samples are downsampled to 24×24, flattened, and projected to 50 dimensions.

This can be interpreted as "losing some information" when performing a Cai-Lim projection: in smaller dimensional spaces, distributions μ and ν seem to be closer than they actually are. This is an inevitable byproduct of any projection operation. Lemma 6.1 implies the following corollary.

Corollary 6.2. *Let $m, n \in \mathbb{N}$ and $p \in [1, \infty]$, and assume $m \leq n$. Consider $\mu, \nu, \rho, \zeta \in M^p(\mathbb{R}^n)$, and pick any $V \in O(m, n)$ and any $b \in \mathbb{R}^m$. Suppose $W_p(\mu, \nu) \geq W_p(\rho, \zeta)$. Then, there exists $\varepsilon > 0$ such that if $W_p(\mu, \nu) - W_p(\varphi_{V,b}(\mu), \varphi_{V,b}(\nu)) \leq \varepsilon$, then*

$$W_p(\varphi_{V,b}(\mu), \varphi_{V,b}(\nu)) \geq W_p(\varphi_{V,b}(\rho), \varphi_{V,b}(\zeta)).$$

Proof. Set $\varepsilon = W_p(\rho, \zeta) - W_p(\varphi_{V,b}(\rho), \varphi_{V,b}(\zeta))$. The result then follows immediately by Lemma 6.1. □

Corollary 6.2 states the following. If we "do not lose too much information" when performing a Cai-Lim projection of the two farthest apart distributions (captured by the assumption that $W_p(\mu, \nu) - W_p(\varphi_{V,b}(\mu), \varphi_{V,b}(\nu)) \leq \varepsilon$), then the inequality $W_p(\mu, \nu) \geq W_p(\rho, \zeta)$ between the original distribution is preserved between their projections.

Figure 4 compares the empirical Wasserstein distance using orthonomal projection compared to Gaussian random projection and sparse random projection when MNIST is perturbed with additive Gaussian noise. Further results can be found in Section C of Supplementary Material. We find that orthonormal projection better preserves distributional information than Gaussian and sparse random projections.

7 RELATED WORK

`SuperStAR` combines various techniques across different fields and integrates them into a unique process for increasing the robustness to semantic-preserving transforms.

Data augmentation for classification robustness. A common technique for increasing the robustnesss of classifiers is data augmentation through the generation of corrupted examples with semantic-preserving shifts [Hendrycks et al., 2019, Erichson et al., 2022, Verma et al., 2019, Yun et al., 2019, Kim et al., 2020, Hendrycks et al., 2020]. Our approach complements such approaches and improves robustness through transformation of corrupted samples to the original data distribution.

Distribution shift detection. Out-of-distribution shift detection has gained significant interest as more machine learning models are deployed into safety critical systems [Kaur et al., 2022, Hendrycks and Gimpel, 2018, Lee et al., 2018]. In [Rabanser et al., 2019], various approaches to dimensionality reduction are explored and empirical results demonstrating the benefit to distribution shift detection are presented. Our work expands on these observations and utilizes a theoretically sound approach of using orthogonal projections for dimensionality reduction.

Deep learning for image restoration. Deep learning approaches for image restoration and recovery from corruption is well studied in the literature and exhaustive review is beyond the scope of this paper. Most of these approaches focus on a specific corruption type or a set of corruptions. For example, Zhang et al. [2017] approaches Gaussian denoising by constructing denoising convolutional feed-forward networks. For a recent survey of deep blurring approaches and comprehensive approaches targeting multiple sets of noises we refer to Zhang et al. [2022], Ledig et al. [2017], Zamir et al. [2021, 2020, 2022]. Such approaches utilize a generative model to restore information lost due to a low resolution. These methods are limited in recovery and can result in image artifacts which degrade classification performance. Here, we attempt to alleviate such limitations by utilizing a composition of transformations which are selected automatically depending on the context. Additionally, the performance can be enhanced with additional image transformations in the action library (see Sec. 8.1).

8 APPLICATION: IMAGENET-C

We now describe the application of our `SuperStAR` algorithm to the ImageNet-C benchmark for distribution shifts [Hendrycks and Dietterich, 2019]. The ImageNet-C dataset is constructed from ImageNet samples corrupted by 19 semantic-preserving transformations. Of these, we target the subset of shifts for which there exists strong prior literature on manual correction. This allows us to construct

an action library with effective individual corrective transformations, a foundation on which we implement our tool for automated online correction. Namely, we target distribution shifts arising due to additive noise (i.e., gaussian, shot, impulse, and speckle noise shift) and modifications to the image histogram (i.e., brightness, contrast, and saturate shift), which we refer to as noise-type and histogram-type shifts, respectively. We evaluate our algorithm on ImageNet classifiers trained with and without various state-of-the-art data augmentation techniques, and we report each classifier's accuracy on ImageNet-C data with and without correction by `SuperStAR` .

8.1 SURROGATE CORRUPTIONS AND ACTIONS

As discussed in Section 5, in practice the corrupting transformations present at test time are unknown to the designer. Hence, surrogate corruptions are necessary at training time. To maximize generalization, we therefore select two surrogate corruptions which subject the images to a broad set of transformations. Below, we describe in greater detail the selection criterion for each class of shift we target.

Additive Noise. We use additive uniform noise, $Uniform(-c, c)$, as a representative of noise-type shifts. We select the severity of this corruption based on the average entropy of the corrupted and uncorrupted data measured by $\mathbb{F}_R$.

Modifications to Image Histogram. We adjust the γ value of the images to create a representative of histogram-type shifts. For this surrogate corruption, we select the severity based on the average brightness of the corrupted and uncorrupted data measured by $\mathbb{F}_R$.

Formally, given a random sample $\mathbf{V}_c$ of the surrogate corrupted data and a random sample $\mathbf{V}$ of ImageNet data, for both surrogates we select the parameter c such that

$$\frac{\mathbb{F}_R(\mathbf{V}_c)_i - \mathbb{F}_R(\mathbf{V})_i}{\mathbb{F}_R(\mathbf{V})_i} \approx 0.60, \tag{6}$$

where $\mathbb{F}_R(\mathbf{X})_i$ denotes the ith index of $\mathbb{F}_R(\mathbf{X})$. For our noise-type and histogram-type shift surrogates, we use $i = 2$ and $i = 0$, respectively. Section D of Supplementary Material shows a sample image subjected to these surrogate corruptions.

We manually select an action library $\mathbb{A}$ of eight correcting transformations. We describe the actions by category below.

Smoothing Transformations. We include a denoising convolutional neural network from the MATLAB Deep Learning Toolbox, a bilateral filter with filter size 2, wavelet denoising with BayesShrink thesholding [Chang et al., 2000], and wavelet denoising with VisuShrink thresholding [Donoho and Johnstone, 1994].

Histogram Equalization Transformations. We use Contrast Limited Adaptive Histogram Equalization (CLAHE) to correct for histogram modifications. (window size, contrast change limit) of (2,1), (2,2), and (6,1).

For each transformations, we select weak parameters to guard against single actions with irreversibly destructive effect. Simultaneously, this allows `SuperStAR` to adapt accordingly to the noise severity. Finally, we include in $\mathbb{A}$ an action that does not enact any transformation, allowing for inaction in the presence of benign corruptions.

8.2 EXPERIMENTAL SETUP

We train a deep neural network policy π with actions $\mathbb{A}$ and surrogate corruptions defined above. Sequences are limited to five actions, but a shorter sequence may occur based on the stopping criteria in Algorithm 1. We choose our stopping condition threshold to be $\alpha = 0.9$ and $\beta = 0.995$.

In constructing our training set of surrogate corruptions, we choose $c = 0.9$ and $\gamma = 3.0$. The neural network policy π is trained using the advantage actor critic algorithm. The details of the network architecture and hyperparameters can be found in Section E of Supplementary Material. Additionally, the reinforcement learning training curves can be found in Section F of Supplementary Material. For the estimation of Wasserstein distances, we convert images to grayscale and project them to 5000 dimensions using a randomly generated orthonormal matrix. Finally, we select the reward hyperparameters $\lambda = 20$ and $\omega = 0.994$.

We deploy the learned policy π in `SuperStAR` to correct noise-type and histogram-type ImageNet-C corruptions, and we evaluate the accuracies of Resnet-50 classifiers with and without correction. We evaluate a baseline classifier trained without data augmentation, as well as classifiers trained with data augmentation through AugMix, NoisyMix, DeepAugment, DeepAugment with Augmix, and Puzzlemix.[3]

8.3 RESULTS AND DISCUSSION

Table 1 summarizes the classifier accuracy improvements from applying `SuperStAR` to noise- and histogram-type shifts from ImageNet-C. Corrections via our `SuperStAR` algorithm leads to accuracy improvements in nearly all cases of shift, with maximum improvement of 14.21% (averaged across all five severity levels) for the baseline classifier evaluated on shot noise data. Further, when combined with data augmentation, `SuperStAR` leads to higher accuracies than `SuperStAR` or data augmentation alone.

Additionally note that when no distribution shift is present, `SuperStAR` refrains from taking any action and does not harm performance. Similarly, on the classes of ImageNet-

[3]Our code can be found at https://github.com/vwlin/SuperStAR.

Table 1: Average accuracies (%) on noise- and histogram-type ImageNet-C shifts with and without SuperStAR for ResNet-50 classifiers. Accuracy improvement is denoted by Δ = recovered − shifted. Values are taken over 5 severity levels with 3 trials each. SuperStAR improves accuracy in almost all cases, with a maximum increase of 14.21% .

	Baseline (No Data Aug.)			AugMix			NoisyMix			DeepAugment			DeepAug+AugMix			PuzzleMix		
shift	**shifted**	**recovered**	**Δ**	**shifted**	**recovered**	**Δ**	**shifted**	**recovered**	**Δ**	**shifted**	**recovered**	**Δ**	**shifted**	**recovered**	**Δ**	**shifted**	**recovered**	**Δ**
none	74.52	74.52	0.00	75.94	75.94	0.00	76.22	76.22	0.00	75.86	75.86	0.00	75.26	75.26	0.00	75.63	75.63	0.00
gauss. noise	31.11	43.44	**12.33**	41.90	50.87	**8.98**	52.71	55.51	**2.80**	59.07	59.48	**0.41**	55.39	61.43	**6.05**	41.48	46.94	**5.46**
shot noise	28.61	42.81	**14.21**	41.78	50.93	**9.15**	51.81	55.38	**3.57**	58.21	58.46	**1.24**	55.76	62.37	**6.61**	37.39	45.56	**7.77**
impulse noise	26.57	39.36	**12.79**	38.78	47.49	**8.71**	50.73	53.37	**2.64**	58.61	58.38	-0.23	55.16	60.67	**5.50**	35.28	42.82	**7.54**
speckle noise	36.09	49.26	**13.18**	50.61	56.94	**6.33**	57.67	60.88	**3.22**	62.21	63.81	**1.59**	60.93	65.66	**4.74**	42.24	51.92	**9.68**
brightness	65.17	65.72	**0.55**	67.35	68.46	**1.11**	68.82	69.87	**1.05**	69.04	69.73	**0.69**	69.42	70.18	**0.76**	69.59	69.67	**0.08**
contrast	35.56	37.70	**2.14**	48.96	49.85	**0.89**	50.37	52.74	**2.37**	44.89	48.23	**3.33**	56.01	57.40	**1.39**	50.56	52.87	**2.30**
saturate	59.00	59.17	**0.17**	61.42	61.89	**0.47**	63.48	64.00	**0.52**	64.59	64.81	**0.22**	65.79	66.12	**0.33**	65.96	65.60	-0.37

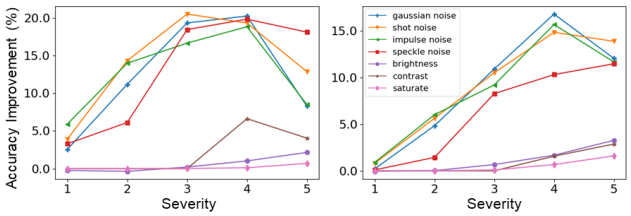

Figure 5: Accuracy improvements for increasing severity evaluated on classifiers trained with (left) no data augmentation and (right) AugMix. In general, performance improvements are more pronounced for greater severities of corruption.

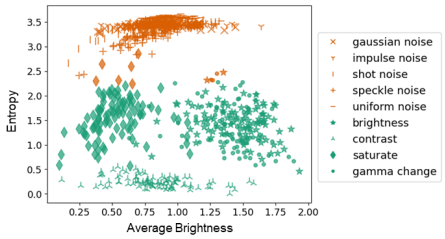

Figure 6: K-means clustering of sampled state representations for noise- and histogram-type shifts from ImageNet-C and our surrogates (projected onto two dimensions). The surrogate shifts are clustered with the appropriate ImageNet-C shifts.

C shifts that we do not target (e.g., blur, weather, etc.), SuperStAR primarily avoids taking action, at worst incurring a 1.80% drop in average accuracy (see Section G of Supplementary Material). For most of these shifts, inaction occurs because there is nothing in the action library that mitigates the shift's effects (in future iterations of SuperStAR, additional actions, such as a superresolution network, can easily be added to the library to handle other classes of shift). However, fog shift is an interesting case where an appropriate action exists (e.g., CLAHE), but it is not taken because our stopping conditions in Algorithm 1 prematurely terminate SuperStAR's procedure. Further discussion can be found in Section H of Supplementary Material.

In Figure 5, we show the accuracy improvements for the baseline and AugMix classifiers at each severity level. In general, accuracy improvements are greater for higher severities, with a maximum improvement of over 20% on shot noise severity level 3 for the baseline classifier. The remaining classifiers exhibit similar trends, as can be seen in Section I of Supplementary Material.

Interestingly, for the hyperparameter selection $\beta = 1.10$ (i.e., allow some increase in Wasserstein distance at each step), we find that SuperStAR selects a non-trivial 5-action sequence of transformations for contrast shift severity level 5, which incrementally increases the accuracy of the AugMix classifier. Figure 2 shows a sample image with the applied transformations and resulting accuracies. The transformations incur a noticeable change in the image.

Overall, our SuperStAR algorithm shows significant improvement in classification accuracy on ImageNet-C for a variety of corruptions. In some cases, SuperStAR identifies complex sequences of corrective transformations. We attribute this strong performance largely to our selection of surrogate shifts. Figure 6 shows the projected state representations for 100 samples of each noise- and histogram-type ImageNet-C shift and each surrogate shift, sorted into $K = 2$ clusters by K-means clustering. The value of K was selected from the range $[1, 9]$ via the elbow method. We see that samples from ImageNet-C noise-type shifts are in the same cluster as those from our uniform noise shift. Likewise, histogram-type shifted samples are clustered with our γ adjustment shift. Thus, SuperStAR generalizes well from the surrogates to these ImageNet-C shifts.

9 CONCLUSION

In this work we presented SuperStAR , an algorithm for distribution shift detection and recovery. The algorithm uses the Wasserstein distance (with a theoretically-sound approach for dimensionality reduction using orthonormal projections) to detect distribution shifts and select recovery actions from a library of image correction techniques. The policy for computing actions is trained using reinforcement learning. We applied our approach to various classifiers on noise- and histogram-type shifts from the ImageNet-C dataset, and we obtained significant accuracy improvements (up to an average 14.21% across all shift severities) when compared the classifiers alone. Expansion of the action library and additional tuning can lead to further improvements on the benchmark.

References

Nicolas Bonneel, Michiel Van De Panne, Sylvain Paris, and Wolfgang Heidrich. Displacement interpolation using lagrangian mass transport. In *Proceedings of the 2011 SIGGRAPH Asia conference*, pages 1–12, 2011.

Yuhang Cai and Lek-Heng Lim. Distances between probability distributions of different dimensions. *IEEE Transactions on Information Theory*, 68(6):4020–4031, 2022.

S Grace Chang, Bin Yu, and Martin Vetterli. Adaptive wavelet thresholding for image denoising and compression. *IEEE transactions on image processing*, 9(9):1532–1546, 2000.

David L Donoho and Jain M Johnstone. Ideal spatial adaptation by wavelet shrinkage. *biometrika*, 81(3):425–455, 1994.

N. Benjamin Erichson, Soon Hoe Lim, Francisco Utrera, Winnie Xu, Ziang Cao, and Michael W. Mahoney. Noisymix: Boosting robustness by combining data augmentations, stability training, and noise injections. *CoRR*, abs/2202.01263, 2022. URL https://arxiv.org/abs/2202.01263.

Dan Hendrycks and Thomas Dietterich. Benchmarking neural network robustness to common corruptions and perturbations. *arXiv preprint arXiv:1903.12261*, 2019.

Dan Hendrycks and Kevin Gimpel. A Baseline for Detecting Misclassified and Out-of-Distribution Examples in Neural Networks, October 2018. URL http://arxiv.org/abs/1610.02136. arXiv:1610.02136 [cs].

Dan Hendrycks, Norman Mu, Ekin D Cubuk, Barret Zoph, Justin Gilmer, and Balaji Lakshminarayanan. Augmix: A simple data processing method to improve robustness and uncertainty. *arXiv preprint arXiv:1912.02781*, 2019.

Dan Hendrycks, Steven Basart, Norman Mu, Saurav Kadavath, Frank Wang, Evan Dorundo, Rahul Desai, Tyler Zhu, Samyak Parajuli, Mike Guo, Dawn Song, Jacob Steinhardt, and Justin Gilmer. The many faces of robustness: A critical analysis of out-of-distribution generalization. *CoRR*, abs/2006.16241, 2020. URL https://arxiv.org/abs/2006.16241.

Leonid Vital'evič Kantorovič. On a problem of Monge. *Zap. Nauchn. Sem. S.-Peterburg. Otdel. Mat. Inst. Steklov. (POMI)*, 312(11):15–16, 2004.

Ramneet Kaur, Kaustubh Sridhar, Sangdon Park, Susmit Jha, Anirban Roy, Oleg Sokolsky, and Insup Lee. CODiT: Conformal Out-of-Distribution Detection in Time-Series Data, July 2022. URL http://arxiv.org/abs/2207.11769. arXiv:2207.11769 [cs].

Jang-Hyun Kim, Wonho Choo, and Hyun Oh Song. Puzzle mix: Exploiting saliency and local statistics for optimal mixup. *CoRR*, abs/2009.06962, 2020. URL https://arxiv.org/abs/2009.06962.

Christian Ledig, Lucas Theis, Ferenc Huszar, Jose Caballero, Andrew Cunningham, Alejandro Acosta, Andrew Aitken, Alykhan Tejani, Johannes Totz, Zehan Wang, and Wenzhe Shi. Photo-Realistic Single Image Super-Resolution Using a Generative Adversarial Network, May 2017. URL http://arxiv.org/abs/1609.04802. arXiv:1609.04802 [cs, stat] version: 5.

Kimin Lee, Honglak Lee, Kibok Lee, and Jinwoo Shin. Training Confidence-calibrated Classifiers for Detecting Out-of-Distribution Samples, February 2018. URL http://arxiv.org/abs/1711.09325. arXiv:1711.09325 [cs, stat].

Stephan Rabanser, Stephan Günnemann, and Zachary C. Lipton. Failing Loudly: An Empirical Study of Methods for Detecting Dataset Shift, October 2019. URL http://arxiv.org/abs/1810.11953. arXiv:1810.11953 [cs, stat].

Aaditya Ramdas, Nicolás García Trillos, and Marco Cuturi. On wasserstein two-sample testing and related families of nonparametric tests. *Entropy*, 19(2):47, 2017.

Vikas Verma, Alex Lamb, Christopher Beckham, Amir Najafi, Ioannis Mitliagkas, David Lopez-Paz, and Yoshua Bengio. Manifold mixup: Better representations by interpolating hidden states. In *ICML*, 2019.

Cedric Villani. *Optimal Transport: Old and New*. Springer Berlin, Heidelberg, 2009.

Z. Wang, A. C. Bovik, H. R. Sheikh, and E. P. Simoncelli. Image Quality Assessment: From Error Visibility to Structural Similarity. *IEEE Transactions on Image Processing*, 13(4):600–612, April 2004. doi: 10.1109/TIP.2003.819861.

Sangdoo Yun, Dongyoon Han, Seong Joon Oh, Sanghyuk Chun, Junsuk Choe, and Youngjoon Yoo. Cutmix: Regularization strategy to train strong classifiers with localizable features. *CoRR*, abs/1905.04899, 2019. URL http://arxiv.org/abs/1905.04899.

Syed Waqas Zamir, Aditya Arora, Salman Khan, Munawar Hayat, Fahad Shahbaz Khan, Ming-Hsuan Yang, and Ling Shao. Learning Enriched Features for Real Image Restoration and Enhancement. In Andrea Vedaldi, Horst Bischof, Thomas Brox, and Jan-Michael Frahm, editors, *Computer Vision – ECCV 2020*, volume 12370, pages 492–511. Springer International Publishing, Cham, 2020. ISBN 978-3-030-58594-5 978-3-030-58595-2. doi: 10.1007/978-3-030-58595-2_30. URL https://link.springer.com/10.1007/

978-3-030-58595-2_30. Series Title: Lecture Notes in Computer Science.

Syed Waqas Zamir, Aditya Arora, Salman Khan, Munawar Hayat, Fahad Shahbaz Khan, Ming-Hsuan Yang, and Ling Shao. Multi-Stage Progressive Image Restoration, March 2021. URL http://arxiv.org/abs/2102.02808. arXiv:2102.02808 [cs].

Syed Waqas Zamir, Aditya Arora, Salman Khan, Munawar Hayat, Fahad Shahbaz Khan, Ming-Hsuan Yang, and Ling Shao. Learning Enriched Features for Fast Image Restoration and Enhancement, April 2022. URL http://arxiv.org/abs/2205.01649. arXiv:2205.01649 [cs, eess].

Kai Zhang, Wangmeng Zuo, Yunjin Chen, Deyu Meng, and Lei Zhang. Beyond a Gaussian Denoiser: Residual Learning of Deep CNN for Image Denoising. *IEEE Transactions on Image Processing*, 26(7):3142–3155, July 2017. ISSN 1941-0042. doi: 10.1109/TIP.2017.2662206. Conference Name: IEEE Transactions on Image Processing.

Kaihao Zhang, Wenqi Ren, Wenhan Luo, Wei-Sheng Lai, Bjorn Stenger, Ming-Hsuan Yang, and Hongdong Li. Deep Image Deblurring: A Survey, May 2022. URL http://arxiv.org/abs/2201.10700. arXiv:2201.10700 [cs].

A PROOF OF THEOREM 5.1

Let us denote by d the pdf of $D_{\mathcal{I}_k \circ \mathbb{T}}$ and by d' the pdf of D . We begin by expanding the definition of $R(\mathcal{I}_k)$.

$$
\begin{aligned}
R(\mathcal{I}_k) &= err(D_{\mathcal{I}_k \circ \mathbb{T}}) - err(D) \\
&= \mathbb{E}_{x_1 \sim D_{\mathcal{I}_k \circ \mathbb{T}}, x_2 \sim D} \left[\mathbb{1}(\mathcal{C}^*(x_1) \neq \mathcal{C}(x_1)) - \mathbb{1}(\mathcal{C}^*(x_2) \neq \mathcal{C}(x_2)) \right] \\
&= \int_{\mathcal{X}} \mathbb{1}(\mathcal{C}^*(x) \neq \mathcal{C}(x))[d(x) - d'(x)]\mathrm{d}x \\
&\leq \left| \int_{\mathcal{X}} \mathbb{1}(\mathcal{C}^*(x) \neq \mathcal{C}(x))[d(x) - d'(x)]\mathrm{d}x \right| \\
&\leq \left| \int_{\mathcal{X}} \left(\sup_{x \in \mathcal{X}} \mathbb{1}(\mathcal{C}^*(x) \neq \mathcal{C}(x)) \right) [d(x) - d'(x)]\mathrm{d}x \right| \\
&= \left| \left(\sup_{x \in \mathcal{X}} \mathbb{1}(\mathcal{C}^*(x) \neq \mathcal{C}(x)) \right) \int_{\mathcal{X}} [d(x) - d'(x)]\mathrm{d}x \right| \\
&\leq \left| \sup_{x \in \mathcal{X}} \mathbb{1}(\mathcal{C}^*(x) \neq \mathcal{C}(x)) \right| \cdot \left| \int_{\mathcal{X}} [d(x) - d'(x)]\mathrm{d}x \right| \\
&\leq \left| \sup_{x \in \mathcal{X}} \mathbb{1}(\mathcal{C}^*(x) \neq \mathcal{C}(x)) \right| \cdot \sup_{A \in \mathcal{A}_{\mathcal{X}}} \left| \int_{A} [d(x) - d'(x)]\mathrm{d}x \right| \\
&= \alpha \cdot d_{TV}(D, D_{\mathcal{I}_k \circ \mathbb{T}}),
\end{aligned}
$$

where $\alpha = |\sup_{x \in \mathcal{X}} \mathbb{1}(\mathcal{C}^*(x) \neq \mathcal{C}(x))|$. The first step assumes that $\mathcal{X}$ is a continuous space. The rest follows from expressing the definition of computing expectation in terms of the classifier error.

B CAI-LIM DISTANCE AND OPTIMAL TRANSPORT

Monge's formulation of the optimal transport problem can be formulated as follows. Let $\mathcal{X}, \mathcal{Y}$ be two separable metric Radon spaces. Let $c : \mathcal{X} \times \mathcal{Y} \to [0, \infty]$ be a Borel-measurable function. Given probability measures μ on $\mathcal{X}$ and ν on $\mathcal{Y}$, Monge's formulation of the optimal transportation problem is to find a transport map $T : \mathcal{X} \to \mathcal{Y}$ that realizes the infimum

$$\inf_{T_\star(\mu)=\nu} \int_{\mathcal{X}} c(x, T(x)) \, \mathrm{d}\mu(x), \tag{7}$$

where $T_\star(\mu) \equiv \mu \circ T^{-1}$ is the pushforward of μ by T.

Monge's formulation of the optimal transportation problem can be ill-posed, because sometimes there is no T satisfying $T_\star(\mu) = \nu$. Equation (7) can be improved by adopting Kantorovich's formulation of the optimal transportation problem, which is to find a probability measure $\gamma \in \Gamma(\mu, \nu)$ that attains the infimum

$$\inf_{\gamma \in \Gamma(\mu,\nu)} \int_{\mathcal{X}\times\mathcal{Y}} c(x, y) \, \mathrm{d}\gamma(x, y), \tag{8}$$

where $\Gamma(\mu, \nu)$ is the set of joint probability measures on $\mathcal{X} \times \mathcal{Y}$ whose marginals are μ on $\mathcal{X}$ and ν on $\mathcal{Y}$. A minimizer for this problem always exists when the cost function c is lower semi-continuous and $\Gamma(\mu, \nu)$ is a tight collection of measures.

Our Cai-Lim distance formulation – equation (5) in the main portion of the paper – can be written as

$$\inf_{\beta \in \Phi^-(\mu,d)} \left[\left(\inf_{\gamma \in \Gamma(\beta,\nu)} \int_{\mathbb{R}^{2d}} \|x - y\|_2^p \, \mathrm{d}\gamma(x, y) \right)^{1/p} \right]. \tag{9}$$

Therefore, (9) is a combination of (7) and (8). To see this, notice that $\mathcal{X} = \mathcal{Y} = \mathbb{R}^d$, and $(x, y) \mapsto c(x, y) = \|x - y\|_2^p$, for some $p \in [1, \infty]$. Hence, the inner part of (9) corresponds to Kantorovich's formulation of the optimal transportation problem. The outer $\inf$, instead, has a Mongenian flavor to it. With this, we mean that the probability measure β must be the one minimizing the p-Wasserstein distance between ν and all the elements in the set $\Phi^-(\mu, d)$ of Cai-Lim projections of μ onto $\mathbb{R}^d$, $d \leq n$. Because

$$\Phi^-(\mu, d) := \{\beta \in M(\mathbb{R}^m) : \varphi_{V,b}(\mu) = \beta, \text{ for some } V \in O(d, n), b \in \mathbb{R}^m\},$$

and $\varphi_{V,b}(\mu) \equiv \varphi^{-1}_{V,b_\star}(\mu) := \mu \circ \varphi^{-1}_{V,b}$ is the pushforward of μ by $\varphi^{-1}_{V,b}$, this reminds us (heuristically) of Monge's formulation. The fact that (9) has a solution is guaranteed by Cai and Lim [2022, Section II].

Some further references can be found at Kantorovič [2004], Villani [2009].

C EMPIRICAL EVALUATION OF ORTHONORMAL PROJECTION

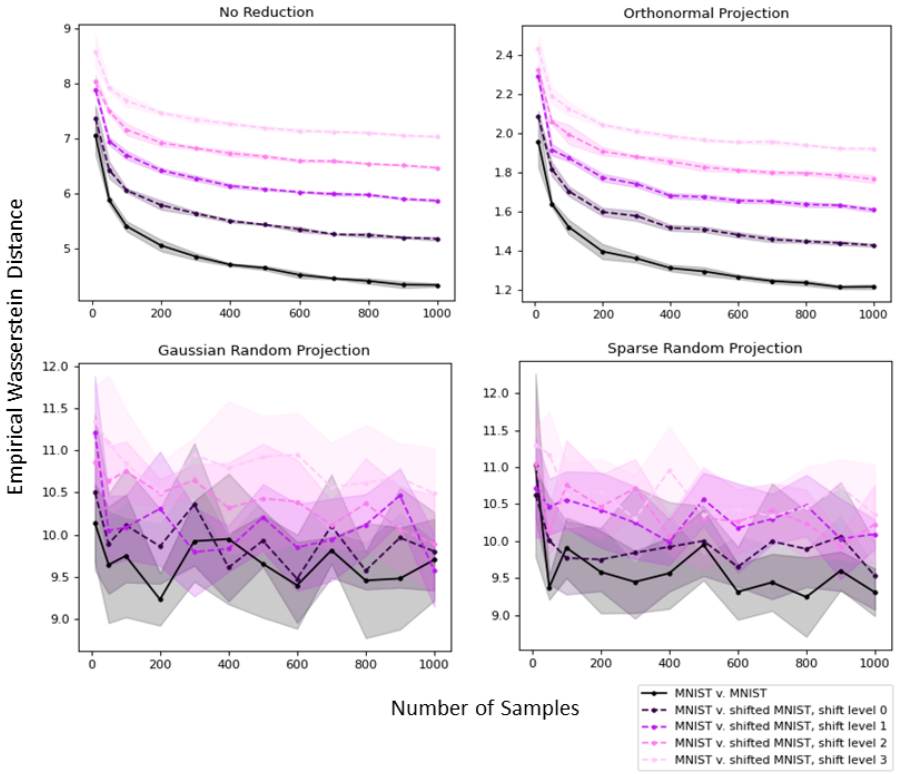

Figure 7: Empirical Wasserstein distance between MNIST and MNIST with varied levels of additive impulse noise, measured over a range of sample sizes. Curves are taken over 5 trials. MNIST samples are downsampled to 24×24, flattened, and projected to 50 dimensions. Orthonormal projection better preserves distributional information than Gaussian random projection and sparse random projection.

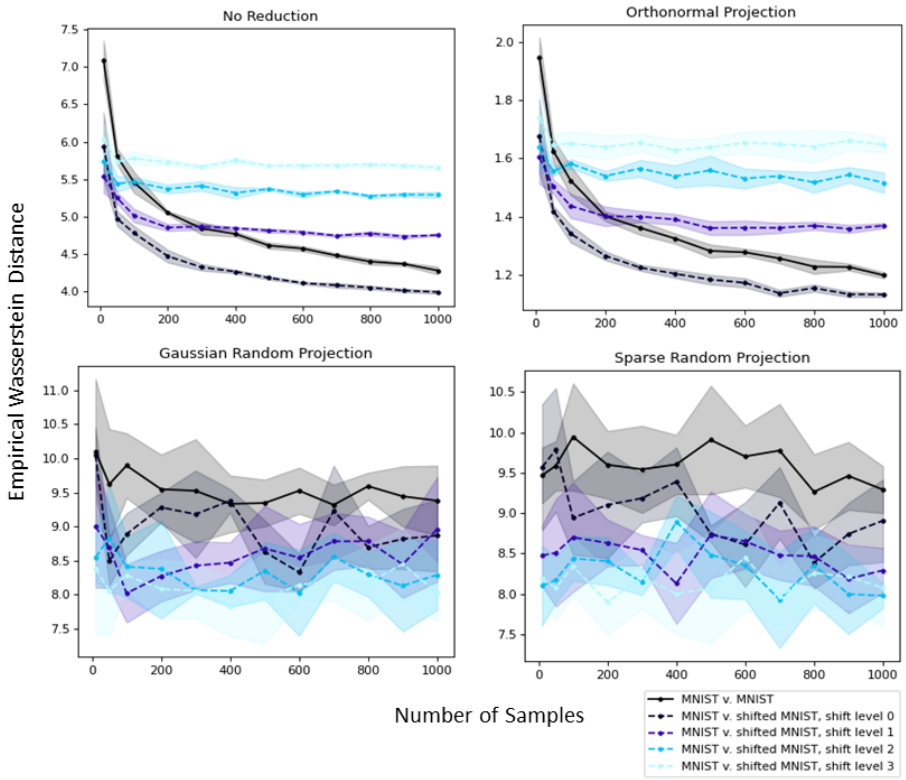

Figure 8: Empirical Wasserstein distance between MNIST and MNIST with varied levels of Gaussian blur, measured over a range of sample sizes. Curves are taken over 5 trials. MNIST samples are downsampled to 24×24, flattened, and projected to 50 dimensions. Orthonormal projection better preserves distributional information than Gaussian random projection and sparse random projection.

D EXAMPLES OF SURROGATE TRANSFORMATIONS

Figure 9: Sample images from ImageNet, ImageNet-C, and clean images subjected to surrogate corruptions.

E REINFORCEMENT LEARNING DETAILS AND HYPERPARAMETERS

For both the actor and critic network, we employ a linear ReLU network with two hidden layers of 128 and 256 units. We train the actor and critic networks until convergence (about 1600 episodes) with learning rate 10^{-4}, learning frequency 1, discount factor 0.9, and exploration rate decaying exponentially from 0.9 to 0.1 according the rule $0.9^{0.07*(episode+1)}$.

F TRAINING CURVES FOR REINFORCEMENT LEARNING

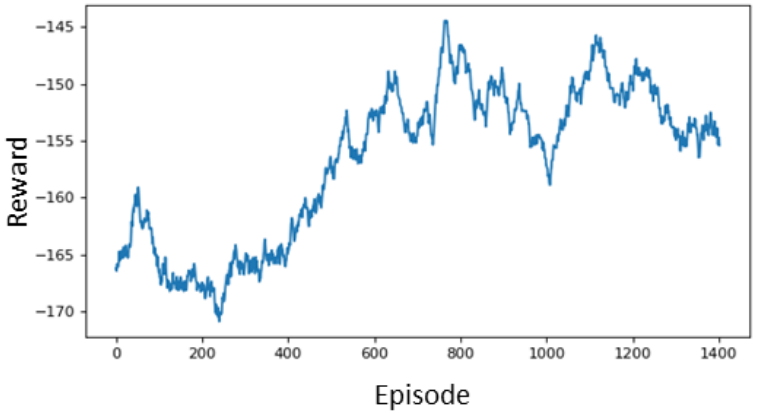

Figure 10: Reinforcement learning training curves, averaged with a moving window of 200 episodes. Values shown are the reward at episode termination.

G SUPERSTAR PERFORMANCE ON ALL IMAGENET-C SHIFTS

Table 2: Average accuracies (%) on each ImageNet-C shift with and without SuperStAR for ResNet-50 classifiers. Accuracy improvement is denoted by Δ = recovered − shifted. Values are taken over 5 severity levels with 3 trials each. On the classes of ImageNet-C shifts that we do not target, SuperStAR primarily avoids taking action.

	Baseline (No Data Aug.)			**AugMix**			**NoisyMix**			**DeepAugment**			**DeepAug+AugMix**			**PuzzleMix**		
shift	**shifted**	**recovered**	**Δ**	**shifted**	**recovered**	**Δ**	**shifted**	**recovered**	**Δ**	**shifted**	**recovered**	**Δ**	**shifted**	**recovered**	**Δ**	**shifted**	**recovered**	**Δ**
none	74.52	74.52	0.00	75.94	75.94	0.00	76.22	76.22	0.00	75.86	75.86	0.00	75.26	75.26	0.00	75.63	75.63	0.00
gauss. noise	31.11	43.44	**12.33**	41.90	50.87	**8.98**	52.71	55.51	**2.80**	59.07	59.48	**0.41**	55.39	61.43	**6.05**	41.48	46.94	**5.46**
shot noise	28.61	42.81	**14.21**	41.78	50.93	**9.15**	51.81	55.38	**3.57**	58.21	58.46	**1.24**	55.76	62.37	**6.61**	37.39	45.56	**7.77**
impulse noise	26.57	39.36	**12.79**	38.78	47.49	**8.71**	50.73	53.37	**2.64**	58.61	58.38	-0.23	55.16	60.67	**5.50**	35.28	42.82	**7.54**
defocus blur	35.21	35.21	0.00	44.48	44.48	0.00	44.72	44.72	0.00	48.10	48.10	0.00	55.52	55.52	0.00	38.02	38.02	0.00
glass blur	25.56	25.56	0.00	32.97	32.97	0.00	35.71	35.71	0.00	38.39	38.39	0.00	44.45	44.45	0.00	25.71	25.71	0.00
motion blur	36.25	36.25	0.00	49.63	49.63	0.00	49.53	49.53	0.00	45.46	45.46	0.00	57.56	57.56	0.00	39.29	39.29	0.00
zoom blur	36.27	36.27	0.00	47.45	47.45	0.00	47.16	47.16	0.00	39.84	39.84	0.00	50.54	50.54	0.00	39.85	39.85	0.00
snow	30.51	29.28	-1.13	37.89	36.85	-1.04	43.20	41.52	-1.68	41.71	39.91	-1.80	47.68	46.36	-1.32	39.48	37.74	-1.75
frost	35.16	35.07	-0.09	41.39	41.24	-0.15	50.05	49.46	-0.59	46.87	46.08	-0.78	51.21	50.26	-0.95	46.96	45.75	-1.21
fog	42.79	42.79	0.00	44.97	44.97	0.00	51.34	51.34	0.00	49.88	49.88	0.00	54.46	54.46	0.00	55.62	55.62	0.00
brightness	65.17	65.72	**0.55**	67.35	68.46	**1.11**	68.82	69.87	**1.05**	69.04	69.73	**0.69**	69.42	70.18	**0.76**	69.59	69.67	**0.08**
contrast	35.56	37.70	**2.14**	48.96	49.85	**0.89**	50.37	52.74	**2.37**	44.89	48.23	**3.33**	56.01	57.40	**1.39**	50.56	52.87	**2.30**
elastic	43.24	43.24	0.00	50.18	50.18	0.00	51.02	51.02	0.00	50.35	50.35	0.00	53.26	53.26	0.00	43.31	43.31	0.00
pixelate	45.51	45.51	0.00	57.25	57.25	0.00	54.23	54.23	0.00	64.31	64.31	0.00	67.31	67.31	0.00	49.03	49.03	0.00
jpeg	52.47	52.47	0.00	58.49	58.49	0.00	61.85	61.85	0.00	56.99	56.99	0.00	61.31	61.31	0.00	56.83	56.83	0.00
speckle noise	36.09	49.26	**13.18**	50.61	56.94	**6.33**	57.67	60.88	**3.22**	62.21	63.81	**1.59**	60.93	65.66	**4.74**	42.24	51.92	**9.68**
gauss. blur	38.08	38.08	0.00	47.17	47.17	0.00	47.30	47.30	0.00	51.93	51.93	0.00	57.53	57.53	0.00	41.07	41.07	0.00
spatter	46.65	46.45	-0.19	53.25	52.97	-0.28	57.63	57.35	-0.29	53.74	53.55	-0.19	57.75	57.64	-0.11	53.27	52.90	-0.36
saturate	59.00	59.17	**0.17**	61.42	61.89	**0.47**	63.48	64.00	**0.52**	64.59	64.81	**0.22**	65.79	66.12	**0.33**	65.96	65.60	-0.37

H INACTION ON FOG SHIFT

As discussed in the main paper, fog shift (a weather-type shift) is a special case of the ImageNet-C shifts classes that we do not target. Although `SuperStAR` chooses to take no action in the presence of fog shift, this is not because there is no appropriate action for this shift. In fact, Contrast Limited Adaptive Histogram Equalization (CLAHE) can achieve a 4.15% accuracy improvement, averaged across all five severity levels, on the AugMix classifier. Further, if allowed to take the full 5-step sequence of actions, `SuperStAR` would initially select a CLAHE action to correct for fog shift. This is supported by Figure 11, which shows that samples from fog shift have a state representation similar to those from our surrogate γ adjustment shift and ImageNet-C histogram-type shifts (i.e., brightness, contrast, and saturate), leading `SuperStAR` to select a similar action for fog shift as for these histogram-type shifts. However, `SuperStAR` uses a stopping condition that can prematurely terminate its procedure. The nature of fog corruption is such that, after taking the first action, `SuperStAR` decides to terminate the process. We speculate that this can be improved by using larger batch sizes for the validation set, which would allow for a more accurate estimate of the Wasserstein distance. Simultaneously, this would come at a higher computational cost for training the RL policy.

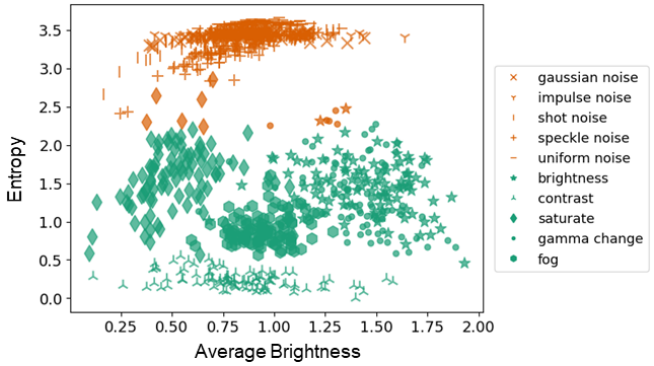

Figure 11: K-means clustering of sampled state representations for noise- and histogram-type shifts from ImageNet-C, fog shift from ImageNet-C, and our surrogates. 100 samples were taken from each shift. $K = 2$ clusters were chosen by selecting K from the range $[1, 10]$ via the elbow method. The projection onto the entropy and average brightness dimensions of the state representation is shown. Samples from fog shift are clustered with γ change shift and the ImageNet-C histogram-type shifts.

I PERFORMANCE ACROSS SEVERITY LEVELS FOR ALL CLASSIFIERS

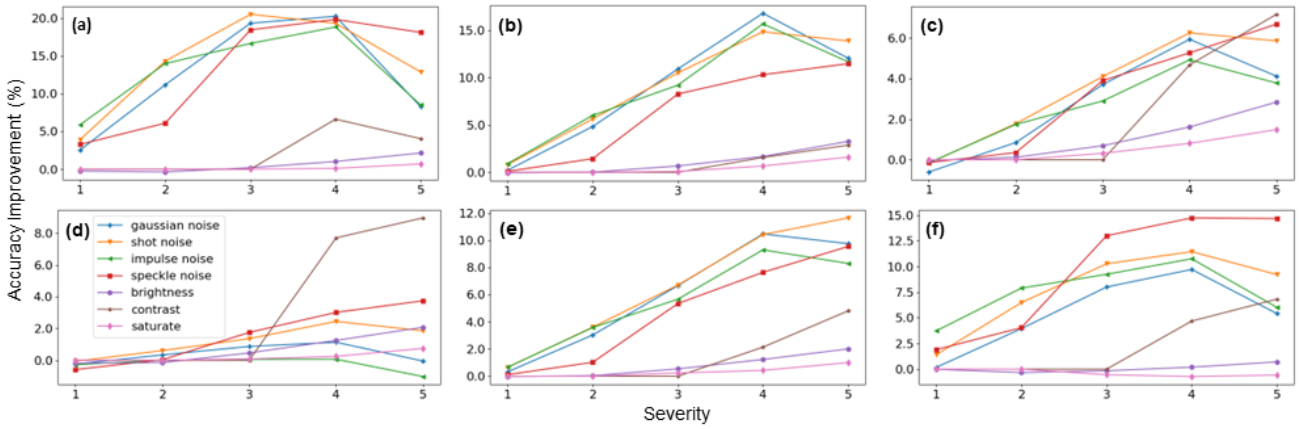

Figure 12: Accuracy improvements for increasing severity evaluated on classifiers trained with a) no data augmentation, b) AugMix, c) NoisyMix, d) DeepAugment, e) DeepAugment and AugMix, and f) PuzzleMix. In general, performance improvements are more pronounced for greater severities of corruption.